Journal of Marine Science and Application (2026) 25: 508-522
https://doi.org/10.1007/s11804-025-00687-4

RESEARCH ARTICLE

Responses of Bow Flare Structures Constructed of Steel, Aluminum Alloy, and GFRP Composite under Extreme Sea Conditions

Bin Liu[1], Lei Zhang[1,2], Yiwen Wang[1], Qingyang Fan[1,2] and C. Guedes Soares[3]

Received: 23 December 2024 / Accepted: 22 January 2025

Abstract

This paper evaluates the responses of equivalent stiffened panels made of steel, an aluminum alloy, and the glass fiber–reinforced plastic (GFRP) composite under extreme slamming loads. These panels are designed for bow flare structures in high-speed crafts. Their equivalence is established with respect to their designs using the same classification society rules. The analysis methods used in this work are illustrated, and slamming loads and inelastic structural responses are analyzed separately. Slamming loads are evaluated using a two-dimensional rigid bow flared section, with dynamic structural deformation and stress responses assessed through nonlinear finite-element analysis. The structures constructed of various materials are verified to meet design requirements. The primary objective of this work is to investigate the safety margin of bow flare structures constructed of steel, an aluminum alloy, and the GFRP composite under extreme sea conditions. The results show that the equivalent composite structures with larger scantlings, particularly the GFRP flat-bar stiffened structure, still exhibit considerably weaker impact strength under extreme slamming loads. The investigation of the structural responses and damage characteristics of equivalent stiffened plates under extreme slamming loads provides a reference for the potential limit state design of the bow flare structures of high-speed crafts.

Keywords Bow flare slamming; Stiffened panel; Steel; Aluminum alloy; GFRP composite; High-speed craft

1 Introduction

High-speed and fast-displacement crafts can be constructed of steel, aluminum alloy, and composite materials (LR, 2020b). Steel remains the most popular material for the construction of such crafts due to its high strength and low cost. The rapid development of aluminum alloy and composite materials has encouraged the use of these materials in hull structures to achieve lightweight special service crafts. Glass fiber–reinforced plastic (GFRPs) composites are widely used for hull construction and are often fabricated using chopped strand mat and woven roving laminates. Aluminum alloys and composites exhibit superior performance over steels because of their lightweight characteristic, which means lessened deadweight, low fuel consumption and emissions, increased passenger and cargo payload, and easy handling.

The behavior of construction materials assists ship designers in the assessment of lifetime structural performance and strength. When high-speed crafts sail under severe sea conditions, their bow structures exhibit significant responses to slamming due to the large vertical relative motions between ships and the water surface. The stiffened plates in bow flare areas are subjected to large impact loads when interacting with seawater. These rapidly varying loads can produce substantial inelastic deformation and structural damage in panels, particularly if these panels are made of aluminum alloys and composites.

The evaluation of the hydrodynamic responses of special service crafts subjected to slamming loads has received increased attention. Slamming loads should be derived accurately for the evaluation of slamming responses (Wang and Guedes Soares, 2017b). Slamming pressure has the

Article Highlights

- The responses of three equivalent stiffened panels under extreme slamming loads are evaluated.
- The equivalent stiffened panels are made of steel, an aluminum alloy, and the GFRP composite.
- The stiffened panels are designed for bow flare structures in high-speed crafts.
- The safety margin of the bow flare structures constructed of different materials is investigated.

✉ Yiwen Wang
yiwenwang90@whut.edu.cn

[1] Green & Smart River-Sea-Going Ship, Cruise and Yacht Research Centre, Wuhan University of Technology, Wuhan 430063, China

[2] School of Naval Architecture, Ocean and Energy Power Engineering, Wuhan University of Technology, Wuhan 430063, China

[3] Centre for Marine Technology and Ocean Engineering (CENTEC), Instituto Superior Técnico, Universidade de Lisboa, Lisbon 1049-001, Portugal

complex nature of a transient impulse with large magnitudes and short durations that moves on hulls rapidly and is distributed unevenly over the contact surface.

The analytical model of slamming loads derived from the Wagner solution focuses on simple geometric shapes, such as two-dimensional (2D) wedge sections, 2D bow flare sections, and three-dimensional (3D) cones (Wang and Guedes Soares, 2014; Korobkin et al., 2014). These analytical models neglect complicated local variation and are therefore unsuitable for complex geometries, such as the ship sections of catamarans and spray rails fitted on fast-displacement crafts. Furthermore, the effects of air entrapment and compressibility are not considered in analytical solutions (Wang and Guedes Soares, 2020). Numerical simulations should be able to analyze slamming on specific structures (Wang and Guedes Soares, 2013; Hong et al., 2017). However, they often require long computation times and accuracy validation and are, therefore, unsuitable in the preliminary design stage. Although the numerical method can ascertain the characteristics of slamming loads, its findings still need to be validated against experimental results. There are two types of experimental techniques generally considered to characterize local slamming loads: seakeeping tests using hydroelastic models of waves (Wang and Guedes Soares, 2016; Mutsuda et al., 2018; Shabani et al., 2019) and free-fall drop tests (Swidan et al., 2016; Wang et al., 2020). However, these experiments are expensive and have high-accuracy requirements for pressure sensors and measurement systems. The measured data are limited since only the location of a sensor's load can be captured. Generally, there are still some limitations and uncertainties in various analysis methods, especially those for the complicated geometries of ships.

The structural responses under slamming loads on high-speed ships are of great importance for guiding the design of ship structures. In practical terms, they are not always in the elastic region, and the maximum stress induced by violent water impact may exceed the limiting stress of materials. Slamming pressures with large amplitudes may lead to local structural damage, especially in cases of extreme waves with high forward speeds. Using analytical solutions and numerical analysis, Yu et al. (2019a, 2019b) focused on the hydroplastic responses of beams and stiffened panels subjected to extreme slamming loads in cases wherein the impact angle is $<5°$. Yang et al. (2018a, 2018b) numerically studied the dynamic ultimate strength of plates and stiffened panels under in-plane loads, which occur at the plating in midship areas subjected to slamming. Only a few experiments have been conducted on hydroplastic responses to slamming in cases wherein large inelastic structural damages are produced. Shin et al. (2018) investigated the structural responses of plates subjected to slamming. The plastic responses of ship sections under extreme slamming have seldom been reported and, therefore, need further investigation.

Wave-induced loads and their respective structural responses are often analyzed separately (Ramos and Guedes Soares, 1998), especially when enormous computation time is required for coupled analysis. The dynamic inelastic responses of plated structures under various rapidly varying loads, such as slamming, sloshing, and green water, have been studied extensively.

The responses of steel and aluminum stiffened panels subjected to dynamic loads have been presented, and finite-element analysis is the preferred tool for predicting structural plastic deformation and failure (Paik and Shin, 2006; Jones, 2013; Khedmati and Pedram, 2014; Cerik, 2017; Wang and Guedes Soares, 2017a; Kang et al., 2025). In numerical modeling, the correct definitions of boundary conditions and material descriptors are important for assessing accurately the impact responses of ship structures. The modeling of boundary conditions should simulate the realistic constraints of the analyzed stiffened panels (Xu et al., 2013). Material nonlinearities and failure criteria should be defined reasonably according to the selected construction materials. The process of material strain hardening to fracture can be well described by a true stress–strain curve representing the basic plastic flow characteristics of materials. However, failure due to material rupture remains poorly resolved numerically because failure strain is highly dependent on the sizes of finite elements (Liu et al., 2017). Given that the material strain rates of stiffened ship panels subjected to slamming loads are small, their effect can be omitted (Liu et al., 2019).

The heat-affected zone (HAZ) phenomenon has to be considered in the analysis of aluminum structures. The act of fusion welding causes the zone adjacent to the weld to anneal slightly, resulting in the loss of strength, which could have an unfavorable effect when stiffened panels are subjected to severe slamming loads. Although the mechanical properties of aluminum alloy materials decrease in the welding HAZ, the experimentally obtained material properties of the HAZ exhibit several inconsistencies (Zha and Moan, 2001; Paik et al., 2006; Liu et al., 2021a). This HAZ phenomenon is also addressed herein when stiffened panels are subjected to slamming impact loads.

Only a few investigations have been performed on the dynamic responses and failure of composite stiffened plates under slamming loads. Most works have mainly focused on the hydroelastic responses of composite structures under water impact (Ojeda et al., 2004; Qin and Batra, 2009; Silva et al., 2020). Hassoon et al. (2017) conducted experimental and numerical analyses to evaluate the inelastic responses and fracture of composite stiffened panels under slamming loads, finding a good agreement between hydrodynamic loads and damage prediction.

The present paper continues the recently reported works of Liu et al. (2020), wherein slamming loads and hydro-

elastic structural responses on the bow flare areas of aluminum fast-displacement crafts were evaluated. Herein, the responses of equivalent stiffened panels made of steel, aluminum alloy, and GFRP composite in bow flare areas are investigated under extreme slamming loads. The equivalence of these panels is established with respect to their designs using the same classification society rules (LR, 2020b). Slamming loads and inelastic structural responses are analyzed separately. The slamming load of a 2D rigid bow flare section is evaluated. Meanwhile, dynamic structural deformation and stress responses are assessed by nonlinear finite-element analysis. The safety margins of the equivalent structures made of different materials are investigated with the comparison of their strengths under design and extreme slamming loads. The equivalent strength concept of different materials is appraised in view of the limit state design of ships.

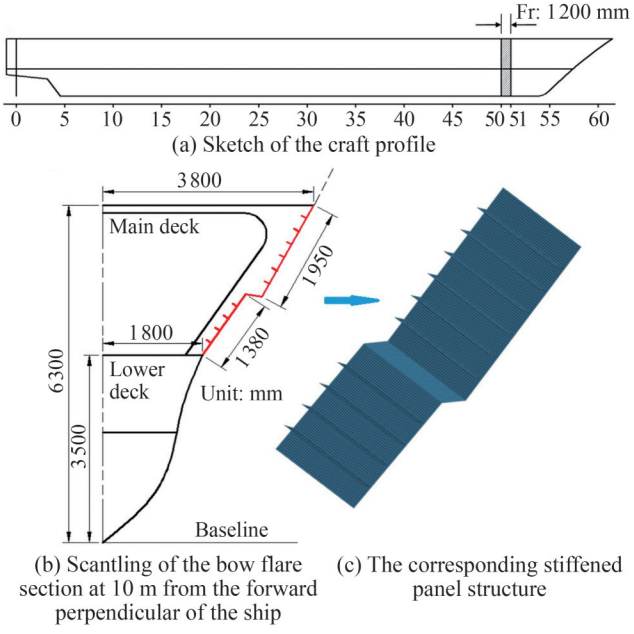

(a) Sketch of the craft profile

(b) Scantling of the bow flare section at 10 m from the forward perpendicular of the ship

(c) The corresponding stiffened panel structure

Figure 1 Schematic of the fast-displacement craft and detailed features of the bow

2 Description of stiffened plates for bow flare areas

Stiffened plates are designed for the bow flare area of a fast-displacement craft 80 m in length. The main particulars of the craft are listed in Table 1, and a sketch of the craft profile and bow flare cross-section at 10 m from the forward perpendicular is given in Figure 1. The stiffened plate has a length of 1 200 mm (Fr: frame spacing) and is restrained at the main and lower decks.

Table 1 Main particulars of the fast-displacement craft

Overall length L_{oa} (m)	80
Length between perpendiculars L_{PP} (m)	70
Breadth B (m)	7.6
Depth D (m)	6.3
Draught T (m)	3.8
Maximum service speed V_s (kn)	30

The primary environmental loading on the stiffened panels in the bow flare area is the slamming load induced by water impact. The plating design pressure at the scantling draft is estimated to be 140 kN/m^2 in accordance with the Rules and Regulations for the Classification of Special Service Craft (LR, 2020b). According to the above rules, structural design criteria can be used to define the thicknesses of hull plates and scantlings of stiffening members on the basis of design pressure, stiffener length and spacing, material properties, and boundary conditions. The structures constructed of steel, an aluminum alloy, and the GFRP composite are designed in reference to "Part 6 Hull Construction in Steel, Chapter 3 Scantling Determination for Mono-Hull Craft", "Part 7 Hull Construction in Aluminum, Chapter 3 Scantling Determination for Mono-Hull Craft", and "Part 8 Hull Construction in Composite, Chapter 3 Scantling Determination for Mono-Hull Craft" in LR (2020b), respectively. Herein, the equivalence among steel, aluminum alloy, and GFRP composite stiffened plates is considered in the design using the same rules under the same design load.

Some advantages and disadvantages of steel, aluminum alloy, and GFRP composite materials are listed in Table 2. The selected materials are mild steel (Grade A), AA5083-H116, and a GFRP laminate, and their mechanical properties given in LR (2020c) are summarized in Tables 3 and 4.

Table 2 Comparison of steel, aluminum alloy, and GFRP composite materials

Material	Advantages	Disadvantages
Steel	Cheap; high strength; high ductility; simple fabrication; easy reparability; fire resistance	Heavy; corrosion; welding distortion
Aluminum alloy	Lightweight; high ductility; no corrosion; easy workability	Expensive; material degradation in the HZA; welding distortion; fatigue; may melt in fires
GFRP composite	Lightweight; easy moldability into complex shapes; ability to tailor properties; no painting or fairing; no rot or corrosion	Low ductility; low fire resistance; toxic fumes

Table 3 Material properties of steel and aluminum alloy

Property	Steel (Grade A)	Aluminum 5083-H116
Young's modulus (GPa)	206	70
Poisson's ratio	0.3	0.33
Yield strength—unwelded (N/mm^2)	235	215
Yield strength—welded (N/mm^2)	235	125
Ultimate tensile strength—unwelded (N/mm^2)	400–520	305
Ultimate tensile strength—welded (N/mm^2)	400–520	275

Table 4 Material properties of different composites

Material properties	CSM450, fc = 0.286	CSM300/600, fc = 0.33	WR800, fc = 0.5
Ultimate tensile strength (N/mm^2)	82	91	190
Tensile modulus (N/mm^2)	6290	6950	14500
Ultimate compressive strength (N/mm^2)	115	122	147
Compressive modulus (N/mm^2)	5400	7200	14000
Ultimate shear strength (N/mm^2)	61	64	78
Shear modulus (N/mm^2)	2730	3000	3290
Poisson's ratio	0.3	0.3	0.092
Thickness (mm)	1.112	0.625/1.250	0.979
Angle (°)	–	–	0.90
Ultimate elongation	–	–	2.0%

The design scantlings of the steel, aluminum alloy, and GFRP composite stiffened plates are given in Table 5 and Figure 2. These scantlings satisfy the minimum requirements for the thickness of platings and section modulus, inertia, and web area of stiffening members in LR (2020b). The scantlings with aluminum alloy 5083-H116 in the bow flare structure of the prototype craft are selected practically (Table 2). Additional details about equivalent design principles can be found in Doan et al. (2020). A composite hat-stiffened panel configuration is considered an alternative to the flat-bar stiffened panel configuration (Figure 2(b)). The geometry of the hat-stiffened panel configuration is also determined with LR (2020b). Figure 3 shows the details of the GFRP composite plates used to fabricate the composite stiffened structures. Generally, composite flat-bar stiffened panels are ideal for simple and low-cost applications where stiffness and load-bearing capacity are not the primary concern. By contrast, composite hat-stiffened panels are suited for high-performance applications wherein strength, stiffness, and load distribution are critical. However, the use of these panels comes at the expense of increased costs and manufacturing complexity.

Table 5 Scantlings of stiffened panels in the bow flare area

Variable	Steel	Aluminum	GFRP
Frame spacing (mm)	1200	1200	1200
Stiffener spacing (mm)	275	275	275
Side shell (mm)	6.0	8.0	8.0
Heavier plate (mm)	10.0	12.0	12.0
Stiffener (mm)	FB 100 × 8	FB 120 × 10	FB 150 × 15/Top-hat stiffener*

Note: * The scantling of the top-hat stiffener is shown in Figure 2(b)

3 Analysis method and technique

Slamming analysis is carried out using the explicit finite-element package LS-DYNA version 971 (Hallquist, 2006). The finite-element method (FEM) is based on an arbitrary Lagrangian–Eulerian (ALE) formulation and a penalty coupling algorithm. The 3D fully coupled ALE/FEM method is the most suitable computing method for analyzing the responses induced by extreme slamming, coupling the deformations of fluid and structures. However, this 3D method has the following limitations: 1) Its calculation is time-consuming, and finding a rational mesh to analyze the full-scale ship structure is difficult. 2) It cannot simulate the fracture of ship structures.

In the present analysis of a full-scale ship structure, the coarsest mesh size has to be approximately 25 mm because the width of the HAZ in welded aluminum stiffened panels has been suggested to be 25 mm (Zha and Moan, 2001; Paik et al., 2005). A coarse mesh cannot simulate the behavior of the HAZ material in aluminum structures. In the present analysis, the mesh of 25 mm generates numerous finite elements (approximately 1.7×10^7) for the 3D numerical model (Figure 5 in Liu et al. (2020)). This situation poses practical challenges to numerical simulation in terms of computing power/time. Therefore, the decoupled approach is the preferred tool for analyzing slamming loads and structural responses separately. 1) Slamming pressures are first estimated using the ALE algorithm, which is based on the 2D rigid body assumption. 2) Structural responses are computed separately using FEM. This method can well simulate structural fracture, which has to be considered in the analysis of structural responses due to extreme slamming.

The hydrodynamic analysis of slamming-induced loads employs the approach reported by Wang and Guedes Soares (2012, 2013) to estimate water impact loads on 2D rigid sections. Structures are modeled in the form of a Lagrangian mesh with a rigid material, whereas fluids are modeled as a multimaterial Eulerian mesh with void materials, allowing equations of state to be considered despite neglecting deviatoric stresses. Fluid–structure coupling is

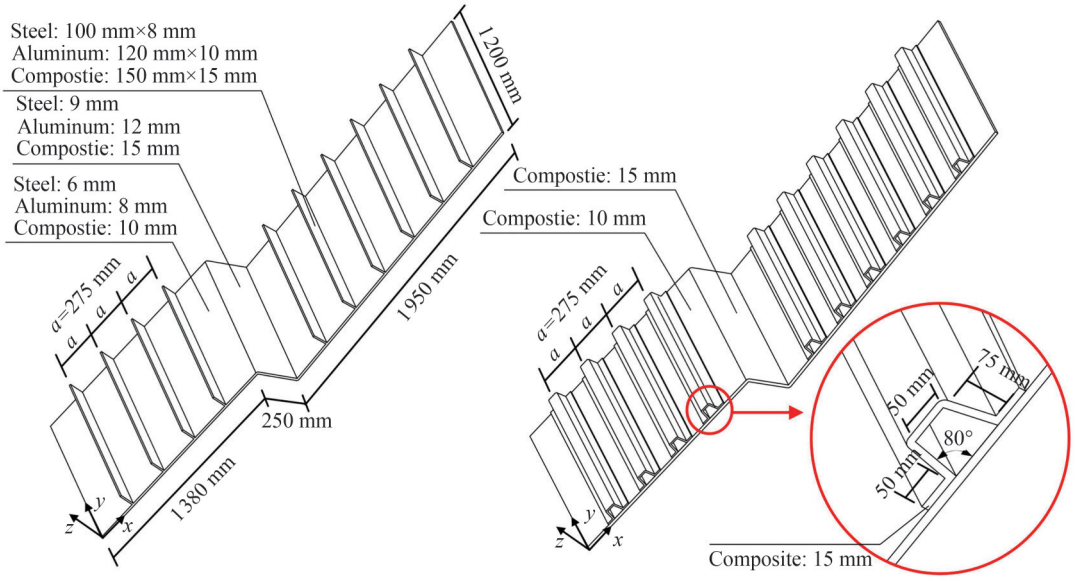

(a) Steel, aluminum, and composite flat-bar stiffened panels (b) Composite hat-stiffened panels

Figure 2 Scantlings of stiffened panels in bow flare areas

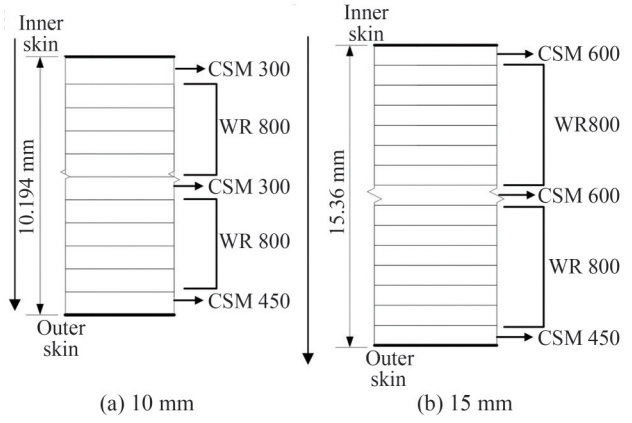

(a) 10 mm (b) 15 mm

Figure 3 Details of composite plates with thicknesses of 10 mm and 15 mm thickness

adopted by the penalty coupling algorithm, which requires a refined selection of related parameters.

The dynamic analysis of structural responses uses the approach reported by Liu et al. (2014, 2015, 2021a, 2021b) to estimate the impact responses of structures. Plates and stiffeners are modeled using four-node shell elements with five integration points throughout their thicknesses, defining the Belytschko–Lin–Tsay shell element formulation. Shell elements can be used in the mechanical analysis of thin-walled structures made of various metals and composite materials. Material properties should be defined reasonably for specific construction materials.

The decoupled method, which analyzes slamming loads and responses separately, was validated against experimental results in the authors' previous investigations. The calculation procedure, particularly the definition of material properties and boundary conditions, was proposed. The decoupled method can predict approximately the response of stiffened panels subjected to extreme slamming loads.

4 Analysis of slamming loads

Stiffened plates are designed in reference to the Rules and Regulations for the Classification of Special Service Craft (LR, 2020b). The corresponding plating design pressure and slamming velocity are 140 kN/m^2 and 9.5 m/s, respectively. In reference to the Rules and Regulations for the Classification of Naval Ships (LR, 2020a), the slamming velocity is approximately 16.6 m/s, indicating that the fast-displacement craft can experience extreme slamming loads in rough seas. Therefore, the slamming velocity of 16.6 m/s is used for the analysis of extreme slamming loading. The analyzed slamming pressures on the ship section are employed as the loads to analyze the response of the bow flare structure under different impact velocities.

4.1 Numerical model

The finite-element modeling of symmetric water entry into a 2D bow flare section is shown in Figure 4. Further explanation about the modeling can be found in Liu et al. (2020). Herein, the rigid cross-section drops vertically into calm water with a constant velocity of 16.6 m/s. Part of the mesh is shown in Figure 5 to illustrate the meshing around the impact domain. The mesh size at the uniform domain area and bow flared section is 25 mm. The domain at the impact region is 6 × (8 + 9.5) m^2, wherein the mesh size is small and uniform to capture the slamming pressure precisely. The fluid mesh size expands moderately toward

the boundary far away from the impact domain to reduce the computation time. The numerical model comprises 470 540 nodes and 234 258 elements. The mesh size in this work is refined compared with that in Liu et al. (2020) (25 mm vs. 50 mm) because a detailed pressure distribution is required for structural analysis.

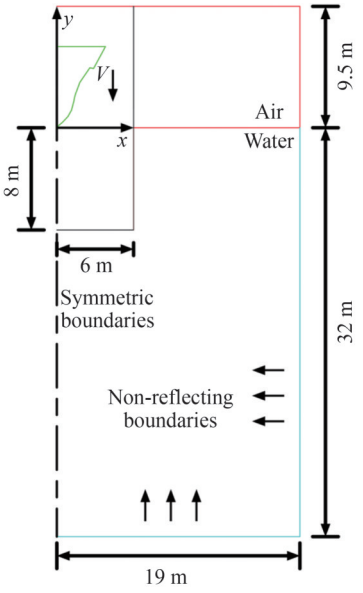

Figure 4 Model setup of symmetric water entry into the 2D bow flare section

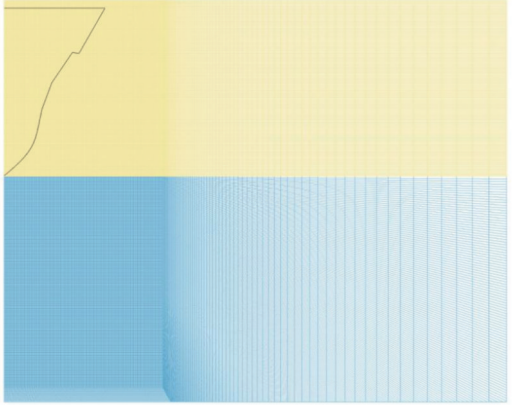

Figure 5 Part of the meshing of the water entry model for the bow flared section

4.2 Slamming pressure results

The maximum pressure contour with an impact velocity of 16.6 m/s is plotted together with free surface elevations (Figure 6(a)). The histories of the slamming pressure of two points at the intersection of the spray rail and lower stiffened plate at the impact velocity of 9.5 and 16.6 m/s are plotted in Figures 6(b) and 6(c), respectively. The instant is set as 0 s when the vertex of the ship section touches the water surface.

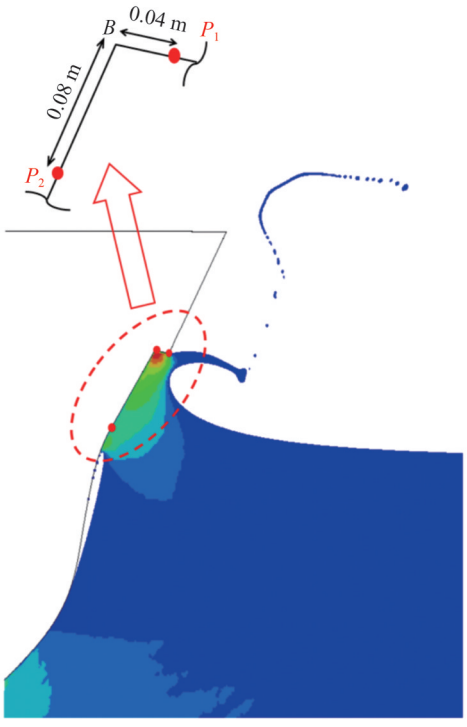

(a) Pressure contour and free surface elevation at the velocity of 16.6 m/s and t = 0.20 s

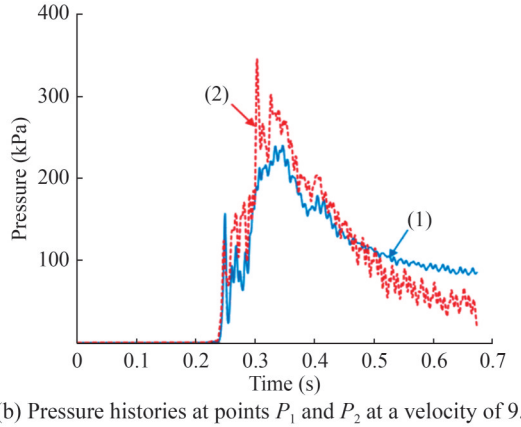

(b) Pressure histories at points P_1 and P_2 at a velocity of 9.5 m/s

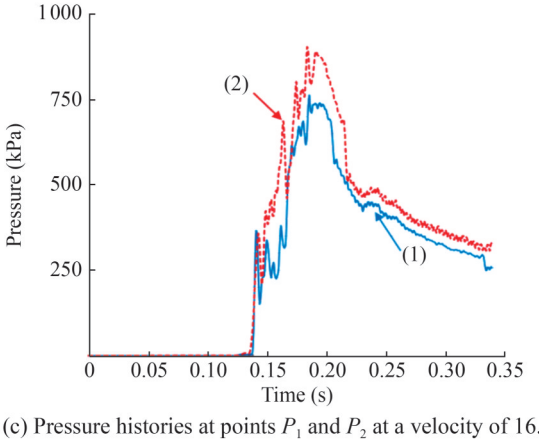

(c) Pressure histories at points P_1 and P_2 at a velocity of 16.6 m/s

Figure 6 Pressure histories at two points on the intersection of the spray rail and lower stiffened plate at different impact velocities

The slamming pressure peak is normally assumed to be proportional to the square of the impact velocity. The pressure peak is expressed as $P_{max} = 0.5\rho C_{Pmax} V^2$, where ρ is the water density, V is the impact velocity, and C_{Pmax} is the coefficient of the maximum pressure assumed to be related to the deadrise angle of the shape only. The maximum instantaneous pressure reaches 903 kPa when the impact velocity is 16.6 m/s and is approximately 2.6 times that when the impact velocity is 9.5 m/s, whereas the impact velocity increases by approximately 1.7 times. Under the impact velocities of 9.5 and 16.6 m/s, C_{Pmax} values of 1.9 and 1.6, respectively, are obtained for point P_2 (Figure 6) and of 1.3 and 1.4, respectively, are acquired for point P_1. Nevertheless, the same C_{Pmax} is considered for each location in the analytical model. As the result of the evolution of the fluid, the jet flow hits the spray rail. This phenomenon is recognized as a secondary impact. The slamming pressure affected by the jet flow appears to be sensitive to the impact velocity. Given the complex nature of the slamming event, assessing the pressure peak with the coefficient of the slamming pressure for the ship section with the spray rail in the extreme environment may be too simple. After the pulse, pressures decrease rapidly after the impulse peak (Figures 6(b) and 6(c)). Although the distance between P_1 and P_2 is only 0.12 m in the ship section, the difference in their time histories of slamming pressures, especially the pressure peak, is obvious. The pressure peak in P_2 is 44% larger than that in P_1 under the design load but decreases to 19% under extreme load (Figures 6(b) and 6(c)). Along the peak amplitude, the slamming pressure histories show different trends under different velocities. The reduction rate of the pressures increases under high impact velocity. As a result of the spray rail, the jet flow sinks and the free surface evolution of such ship section's impact is different from that of a conventional ship.

The distribution of slamming pressures under the impact velocities of 9.5 and 16.6 m/s is presented in Figures 7(a) and 7(b). The pressure peak concentrates around the corner of the spray rail, indicated as point B in Figure 6(a). However, after the maximum impulse occurs, the pressures on area AB become considerably higher than those on BC. Therefore, the structural responses and deformation of area AB under extreme slamming loads are analyzed as discussed in Section 5. Considering the characteristics of slamming loads, evaluating the impact strength of slamming loads as a simplified, spatially uniform distributed pressure and neglecting the variation in time and location, especially for ships with spray rails, are inappropriate.

5 Analysis of structural responses under slamming loads

The responses of the bow flare structure under design and extreme slamming loads are analyzed. The time history of slamming pressure obtained from hydrodynamic analysis (Section 4.2) is the loading input. Dynamic pressure–time curves are applied at the spray rail (area BC) and the stiffened plate below the spray rail (area AB) and are distributed uniformly along the length defined by the frame spacing (1.2 m). Structural deformation and stress are then analyzed.

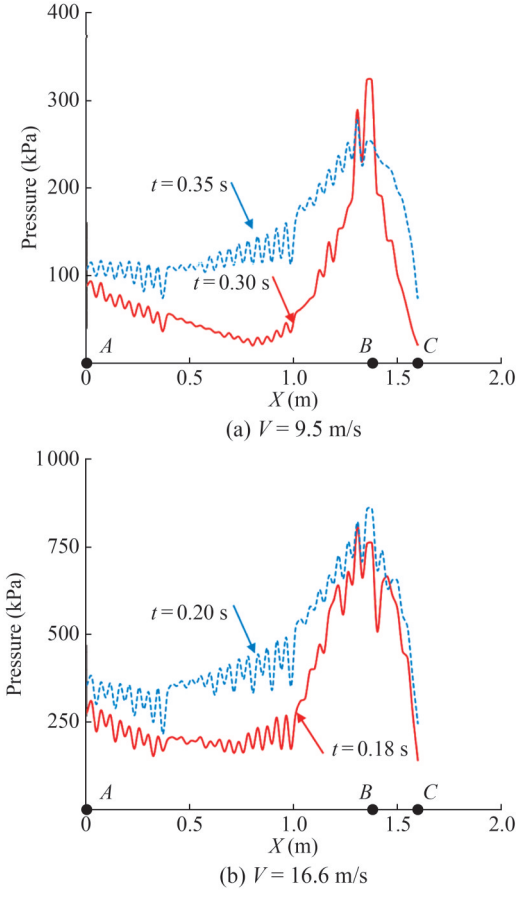

Figure 7 Pressure distribution along the section around the chine

5.1 Finite-element models

The finite-element models in Figure 8 represent the geometries of the stiffened plates in Figure 2. The four edges of the plates and ends of the stiffeners are fully restrained because the primary supporting members are considered to not suffer bending deformations. The 25 mm mesh comprises 12 elements between the longitudinals, and this mesh can well describe the deformation shape of a stiffened panel. The definitions of the material properties of steel, aluminum alloy, and the GFRP composite are presented in the following subsections.

5.1.1 Steel

The definition of material plastic hardening is required in the structural response analysis of steel materials. The material model selected from the library of LS-DYNA is

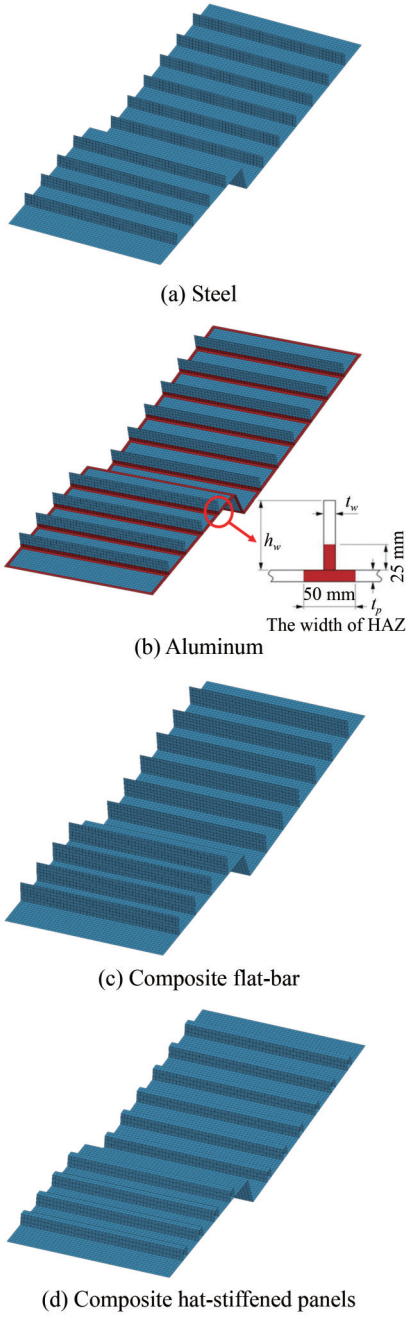

Figure 8 Finite-element model

Mat.24-Piecewise Linear Plasticity, which allows the definition of a true stress–strain curve as an offset table.

The true stress–strain of materials is characterized by the power law relation $\sigma_t = K\varepsilon_t^n$, where the strength coefficient (K) and strain hardening exponent (n) are determined from equations that require only the material yield and ultimate tensile stresses as input (Liu et al., 2017). The material parameters K and n can be determined when the yield stress (σ_y) and ultimate tensile stress (σ_{uts}) are known:

$$\sigma_y = K \cdot 0.006^n \tag{1}$$

$$\sigma_{uts}(1+n) = K\left[\ln(1+n)\right]^n \tag{2}$$

Later, the true stress is determined by the power law relation $\sigma_t = K\varepsilon_t^n$, where $\varepsilon_t > 0.006$. The analyzed true stress–strain curve of mild steel (Grade A) is plotted in Figure 9.

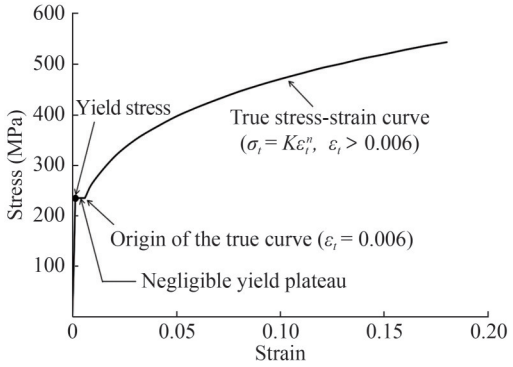

Figure 9 True stress–strain curve of mild steel

5.1.2 Aluminum alloy

The method for defining the mechanical properties of the base material of aluminum 5083-H116 is similar to that used for the steel material (Figure 10).

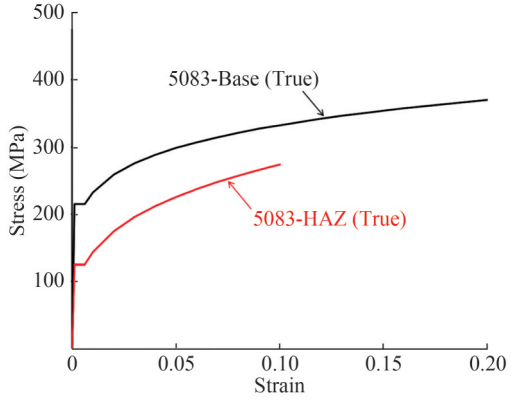

Figure 10 True stress–strain curves of 5083-H116 aluminum alloy at the base and HAZ

For the aluminum-alloy stiffened panel, the HAZ at welded areas is accounted for in the simulation by decreasing the material properties in the HAZ. This approach is necessary when simulating aluminum stiffened plates because the weld decreases the resistance of stiffened plates (Paik et al., 2006). The reduction factor of yield stress due to weld softening at the HAZ is taken as 0.67 (Benson et al., 2013; Cerik, 2017). The knockdown factor is not only applied to the yield strength but also to the entire true stress–strain curve of the 5083-H116 material (Table 3 and Figure 10). In this study, the width of the HAZ is taken as 25 mm.

5.1.3 GFRP composite

The definition of the GFRP composite material differs from those of steel and aluminum materials. The material model selected from the library of LS-DYNA is Mat.54-Enhanced Composite Damage, which is used specifically to deal with arbitrary orthotropic materials, such as composite laminate. In this material model, a minimal amount of input parameters must be specified, and the Chang–Chang failure criterion is used to simulate the ply-by-ply failure of composites (Hallquist, 2006). This material model allows defining each ply by an integration point. The Mat.54 model has been tested and used by numerous previous studies for simulating GFRP composite (Osborne, 2012; Feraboli et al., 2011; Wang et al., 2018).

The GFRP composite panels comprise CSM and WR materials, and their material properties are summarized in Table 4 and Figure 11. These parameters are estimated using the fiber content (fc) of the CSM and WR materials given in LR (2013, 2020b, 2020c). The fiber content is used to describe the properties of composite materials. Similar material parameters were also used by Lu et al. (2019) to analyze the strength of top-hat stiffened composite structures. In the present study, the additional reinforcement at the composite joint with large thickness is ignored to assess structural strength conservatively.

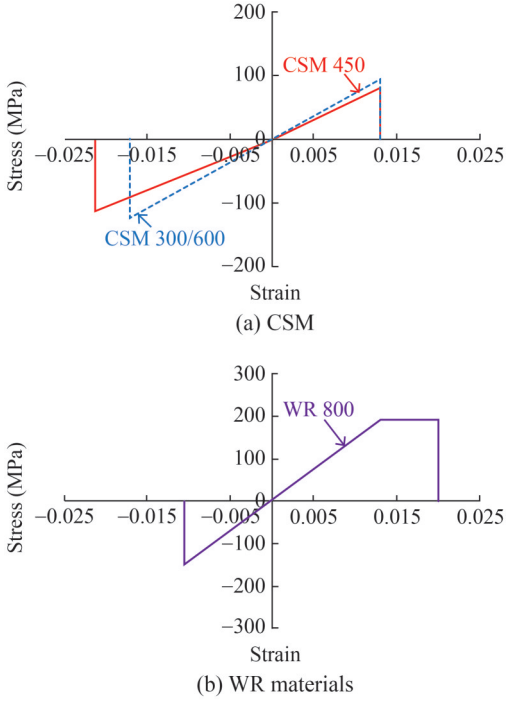

Figure 11 Stress–strain curves of the MAT54 material model with the estimated values given in Table 4

5.2 Finite-element results

As the plating of the spray rail is strengthened, the stiffened plate below the spray rail is the main object of investigation. Thus, in the following subsections, other structures are hidden to illustrate the numerical results well.

5.2.1 Results under the design load

The nominal limiting stress requirements for the plating and primary and secondary stiffening members subjected to local loading conditions are given in terms of limiting stress coefficients (LR, 2020b). These coefficients are expressed as a portion of the 0.2% proof stress of the steel and aluminum materials and the ultimate tensile and the ultimate shear strengths of the GFRP composite material (Tables 6 and 7). Compared with those of the composite panels, the analyzed bending stress coefficients of the steel and aluminum stiffened panels are much closer to the limiting values; nevertheless, the opposite phenomenon is observed for shearing stress. Generally, equivalent design by LR rules with different materials shows the discrepancy of the safety margin in view of the analyzed stresses. Compared with the flat-bar panel, the composite top-hat stiffened panel has higher strength, showing smaller analyzed stresses.

Table 6 Stress coefficient of steel and aluminum structures

Item	Limiting stress coefficient*		Analyzed results			
			Steel		Aluminum	
	Bending	Shear	Bending	Shear	Bending	Shear
Shell plating	0.85	–	0.38	–	0.46	–
Secondary stiffening	0.75	0.75	0.69	0.37	0.75	0.42

Note: *See LR (2020b)

Table 7 Stress fractions in composite structures

Variable	Limiting stress fraction*		
	Tensile, 0.33	Compressive, 0.33	Shear, 0.33
Flat-bar stiffened	0.23	0.30	0.31
Hat-stiffened	0.22	0.15	0.19

Note: *See LR (2020b)

The plots of the maximum bending and shear stresses of the four stiffened panels are presented in Figure 12. The maximum stresses occur at the stiffener's ends. The values of the tensile/compressive stress are similar to those of the bending stress in the cases of composite panels. The first peak stress (at 0.34 s) corresponds to the maximum slamming pressure (Figure 6(b)), whereas the second peak stress (at 0.41 s) is due to continuous loading on the stiffened plate. The GFRP composite stiffened panels, especially the hat-stiffened panel, show small stresses under impact load due to their high plate thickness.

The limiting span: deflection ratio, i.e., the length: midpoint deflection, is used in the assessment of deflection in LR (2020b). The results are summarized in Table 8. In

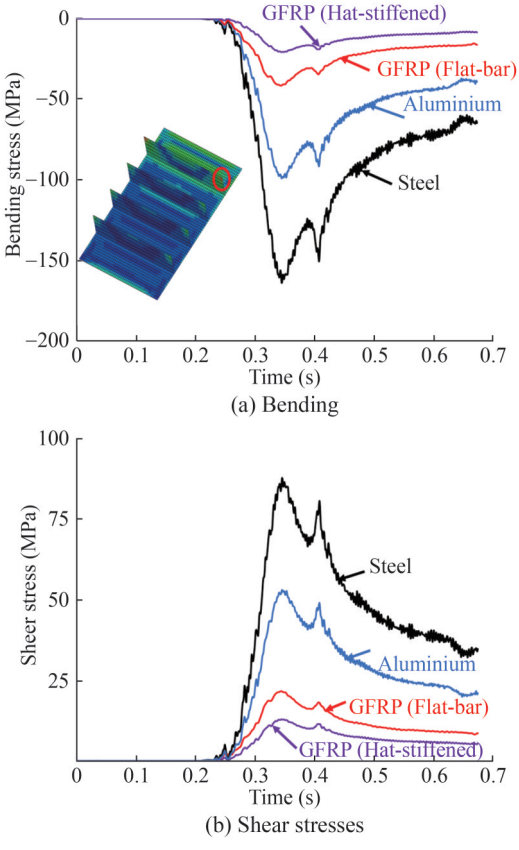

Figure 12 Comparison of the maximum stresses of steel, aluminum, and composite stiffened panels under the design load (V = 9.5 m/s)

Table 8 Deflection in steel, aluminum, and composite structures

Variable	Limit deflection ratios*	Actual deflection ratios
Steel	800	857
Aluminum	475	652
GFRP flat-bar stiffened	150	187
GFRP hat-stiffened	150	202

Note: *See LR (2020b)

structural design with different construction materials, different deflection ratios are used to assess the allowable structural deformation. The ratio of specific modulus, i.e., Young's modulus divided by density, of steel, aluminum, and composite materials is 1 : 0.99 : 0.37. The stiffened panels made of different materials with equivalent design based on LR rules have different bending stiffness values. The plots of the maximum deflections of the four stiffened panels are presented in Figure 13. The maximum deflection occurs at the plating element between longitudinals, the midspan of the stiffened plate below the spray rail, and 0.41 s. The maximum deflection is delayed by a certain amount of time depending on the duration of the slamming loads. Compared with other panels, the GFRP composite stiffened panels, especially flat-bar panels, show much larger deflections under impact load due to their smaller Young's modulus.

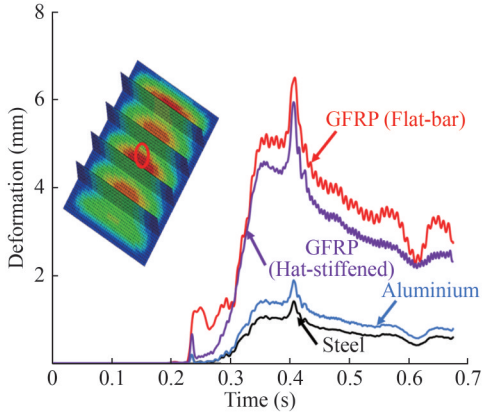

Figure 13 Comparison of the maximum deformation of steel, aluminum, composite flat-bar stiffened, and composite hat-stiffened panels under the design load (V = 9.5 m/s)

In general, all the analyzed stresses and deflections are smaller than the corresponding limiting values, demonstrating that structural design using the three construction materials is reasonable. This finding indicates the equivalence of the stiffened structures made of different materials.

5.2.2 Results under extreme load

The stiffened panels suffer large stresses and deflections under extreme slamming loads. The progressive deformation and failure of the four stiffened panels are summarized herein.

In general, the steel and aluminum stiffened panels experience similar structural deformation processes (Figure 14). Initially, the panels undergo bending deformation under slamming pressure, and the maximum stresses concentrate at the lower stiffener's ends with plastic deformation (t = 0.134 s). As water impacts the panel, the location of the maximum slamming pressure moves upward and the magnitude of pressure increases. Afterward, stresses concentrate at the upper stiffener's ends with large plastic deformation (t = 0.176 s). Plastic deformation develops continuously until the slamming pressure decreases (t = 0.203 s).

Ultimately, although the HAZ effect is considered in the aluminum case (Figure 15), the steel stiffened panel suffers considerably larger plastic strain than the aluminum panel (0.038 vs. 0.020), mainly because the section moment of inertia of the aluminum stiffened panel is 2.08 times that of the steel panel. Generally, compared with the aluminum stiffened panel, the lightweight aluminum stiffened panel has a substantially larger safety margin under extreme slamming loads.

The deformation and failure of the GFRP composite flat-bar stiffened panel are shown in Figure 16. Herein, the damage parameter is selected to illustrate the failure state

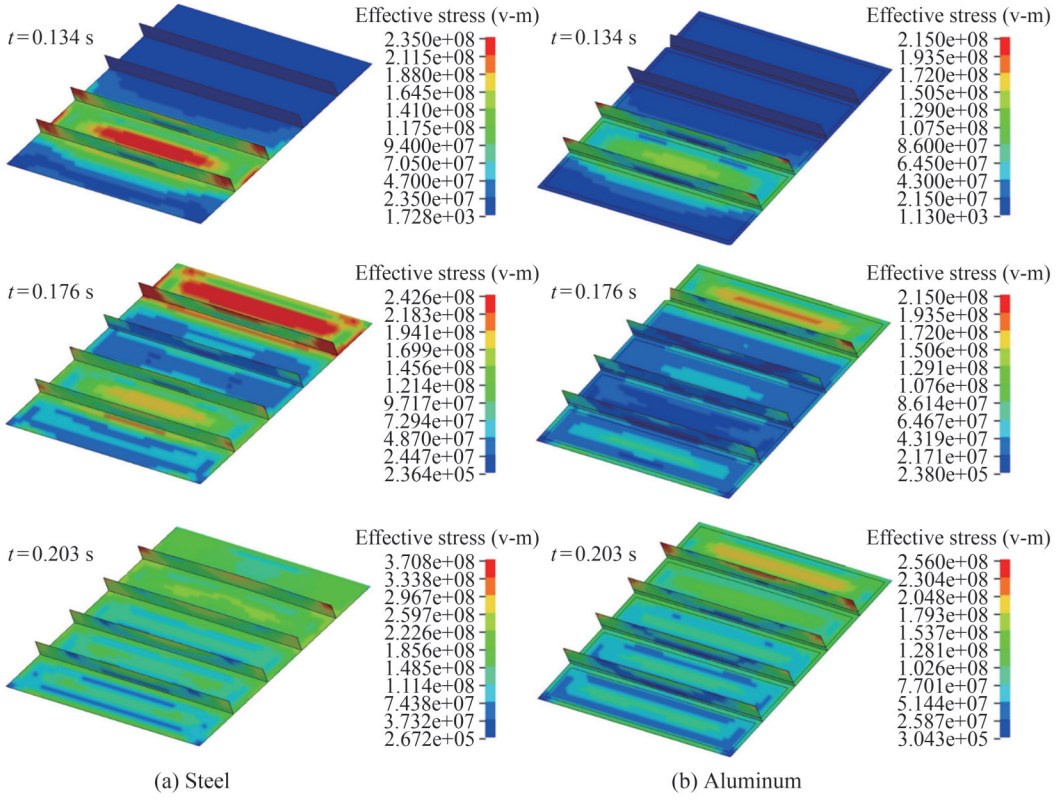

Figure 14 Deformation and failure of stiffened panels

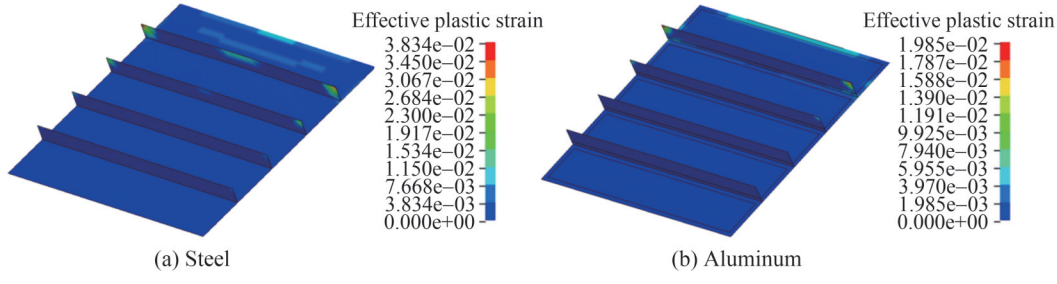

Figure 15 Permanent plastic strain in stiffened panels

of the composite material, and its value ranges from 1, which represents the undamaged state, to 0, which represents the fully damaged state. In the case of the flat-bar stiffener, the panel fails at the lower stiffener's ends first due to the low ductility of the composite material (t = 0.140 s). Afterward, material failure occurs at the upper stiffener's ends. This stiffener then suffers large beam bending deformation and fractures at its free edge (t = 0.198 s). The damage at the midspan is caused by the excessive elongation of the material, and failure at both ends is induced by compression. Subsequently, the fracture propagates rapidly from the stiffener to the attached plate (t = 0.200 s). Finally, the stiffened panel collapses totally at its midspan (t = 0.203 s).

The GFRP composite hat-stiffened panel suffers slight structural damage due to its large section modulus (Figure 17). In contrast to that of top-hat stiffeners, the design of top-hat stiffeners avoids penetrating fracture in the stiffened structure. Only some plies fail at the upper stiffener's ends without the overall fracture of laminates, mainly because the ultimate compressive strength of WR laminates is lesser than the ultimate tensile strength (Table 4). Moreover, given that the top of the hat stiffener has a small section modulus, increasing its thickness is an effective way to increase structural strength. Generally, this design for composite structures provides a similar safety margin as that for steel and aluminum cases.

The plots of the maximum bending and shear stresses of the four stiffened panels under extreme loadings are presented in Figure 18. The maximum stresses also occur at the upper stiffener's ends at 0.20 s. Comparing the two composite cases reveals that the hat-stiffened panel experiences about 19% smaller maximum stresses than the flat-bar panel. This value indicates the safety margin of the hat-

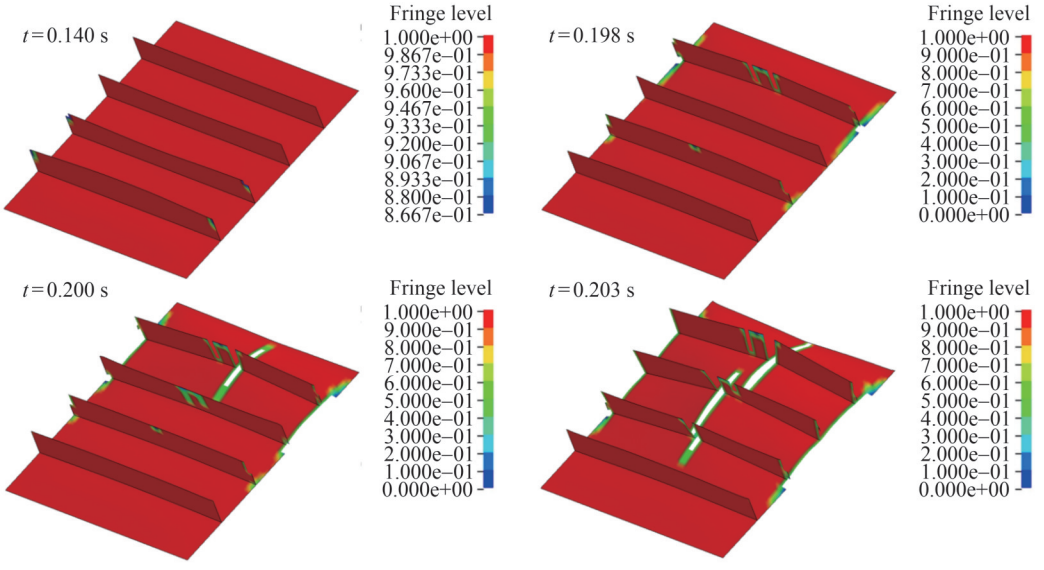

Figure 16 Deformation and failure of the GFRP flat-bar stiffened panel

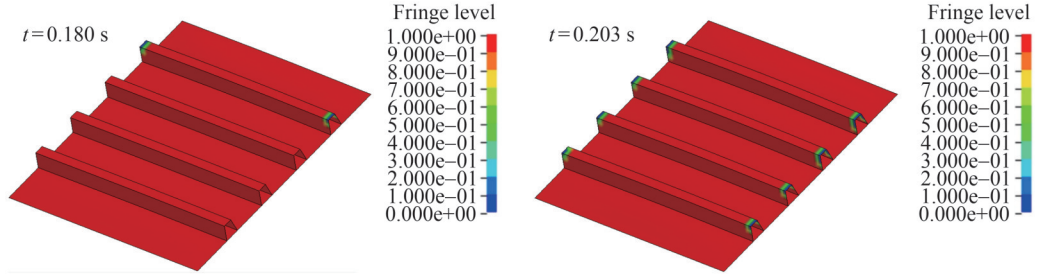

Figure 17 Deformation and failure of the GFRP hat-stiffened panel

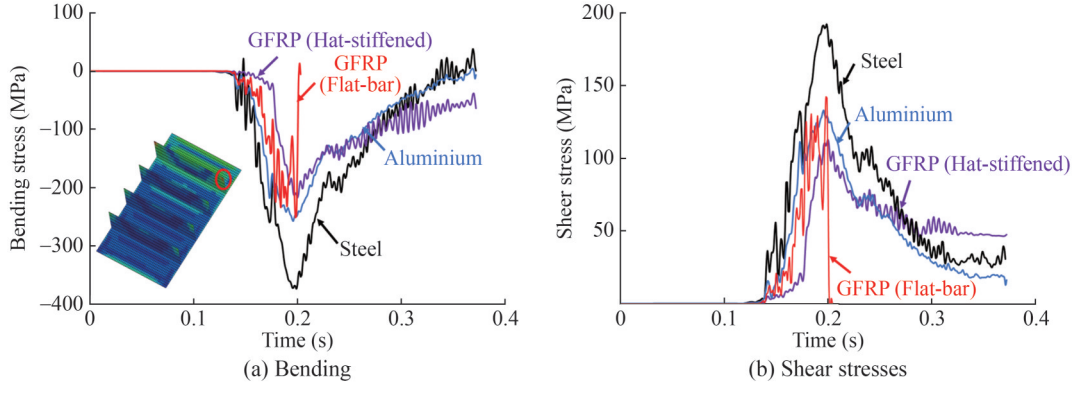

Figure 18 Comparison of the maximum stresses of steel, aluminum, and composite stiffened panels under extreme load ($V = 16.6$ m/s)

stiffened panel. Generally, the analyzed stresses are considerably larger than the allowable design stresses.

The histories of the maximum deflection vs. time are plotted in Figure 19. The maximum deformation occurs at the plate component close to the spray rail. This location differs from that under the design load (Figure 13) mainly because local tensile deformation leads to a large deflection of the stiffened panel. The maximum deformation occurs at the same time as the maximum slamming pressure. In contrast to the result obtained under the design load, the maximum deformation of the steel stiffened panel is 1.68 times that of the aluminum panel (Figure 13) because the steel material experiences larger plastic strain than the aluminum material despite having a larger Young's modulus.

5.2.3 Material selection for ship hulls

In the present study, the weight ratio of the steel, aluminum alloy, composite flat-bar, and hat-stiffened panels is

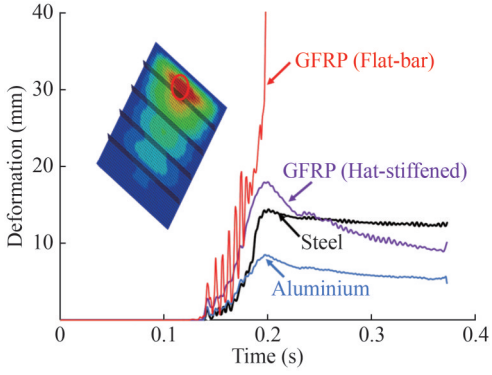

Figure 19 Comparison of the maximum deformation of steel, aluminum, composite flat-bar stiffened, and composite hat-stiffened panels under extreme load (V = 16.6 m/s)

1 : 0.47 : 0.38 : 0.49. Aluminum alloys and the GFRP composite have advantages as shipbuilding materials because of their lightweight structures.

Steel and aluminum alloy are ductile materials that can suffer much larger plastic deformation under extreme loadings compared with other materials. The HAZ effect on aluminum alloy has decreased with the development of manufacturing technology, thus benefiting the use of aluminum alloy in ship hulls. The use of high-strength steel and aluminum alloy as shipbuilding materials has matured in view of the structural strength and fabrication of these materials.

The equivalent composite structure often suffers large bending deformation due to the small tensile modulus of the composite material. The composite stiffened panel experiences earlier fracture than the equivalent steel and aluminum panels due to the brittleness of the composite material. Moreover, the design and fabrication of adhesive joints are far more complicated than those of composite laminates. Therefore, the selection of the composite material for ship hulls should be done with caution. However, with the development of material technology, high-performance composite materials still have potential applications in the marine industry.

6 Conclusion

The response of equivalent stiffened panels made of steel, an aluminum alloy, and the GFRP composite under extreme slamming loads are analyzed and compared by investigating their structural stresses and deformations. This approach illustrates the safety margin of bow flare structures constructed of different shipbuilding materials. The results of this work show that among the three shipbuilding materials, aluminum alloy has the best performance because of its strength and lightweight structure.

Nevertheless, the equivalent composite structures with large scantlings, especially the GFRP flat-bar stiffened structure, still exhibit weak impact strength under extreme slamming loads. The equivalent strength concept of different materials is poorly reflected in the limit state design of ships.

The spray rail design results in the lower stiffened panel experiencing large slamming pressures during water impact. Stresses mainly concentrate at the ends of longitudinal stiffeners passing through web frames, an area that is commonly affected by the processing techniques of aluminum alloy and composite materials. In contrast to that under the design load, the location of maximum deformation moves upward in the stiffened panels under extreme load.

Nomenclature

B	Breadth (m)
$C_{P\max}$	Coefficient of maximum pressure
D	Depth (m)
fc	Fiber content by weight
K	Strength coefficient (MPa)
L_{oa}	Overall length (m)
L_{PP}	Length between perpendiculars (m)
n	Strain hardening exponent
P_{max}	Pressure peak (kPa)
T	Draught (m)
t	Time instance during impact (s)
V	Impact velocity (m/s)
V_s	Service speed (kn)
ρ	Water density (kg/m)
σ_y	Yield stress (N/mm)
σ_{uts}	Ultimate tensile stress (N/mm)
ε_t	True strain

Competing interest C. Guedes Soares is one of Editors for the Journal of Marine Science and Application and was not involved in the editorial review, or the decision to publish this article. Bin Liu is editorial board members for the Journal of Marine Science and Application and were not involved in the editorial review, or the decision to publish this article. All authors declare that there are no other competing interests.

References

Benson S, Downes J, Dow RS (2013) Load shortening characteristics of marine grade aluminium alloy plates in longitudinal compression. Thin Walled Struct 70: 19-32. https://doi.org/10.1016/j.tws.2013.03.002

Cerik BC (2017) Large inelastic deformation of aluminium alloy plates in high-speed vessels subjected to slamming. J. Mar. Sci. Technol 22(2): 1-12. https://doi.org/10.1007/s00773-017-0446-4

Doan VT, Liu B, Garbatov Y, Wu W, Guedes Soares C (2020) Strength assessment of aluminium and steel stiffened panels with openings on longitudinal girders. Ocean Eng 200: 107047. https://doi.org/10.1016/j.oceaneng.2020.107047

Feraboli P, Bonnie W (2011) LS-DYNA MAT54 modelling of the axial crushing of a composite tape sinusoidal specimen. Compos Part A-Appl S 42(11): 1809-1825. https://doi.org/10.1016/j.compositesa.2011.08.008

Hallquist JO (2006) LS-DYNA theory manual. Livermore Software Technology Corporation, Livermore

Hassoon OH, Tarfaoui M, Alaoui AEM, Moumen AE (2017) Experimental and numerical investigation on the dynamic response of sandwich composite panels under hydrodynamic slamming loads. Compos. Struct 178: 297-307. https://doi.org/10.1016/j.compstruct.2017.09.058

Hong SY, Kim KH, Hwang SC (2017) Comparative study of water-impact problems for ship section and wedge drops. Int. J. Offshore Polar Eng 27(2): 123-134. https://doi.org/10.17736/ijooe.2017.jj582

Jones N (2013) Damage of plates due to impact, dynamic pressure and explosive loads. Lat. Am. J. Solids. Struct 10: 767-780. https://doi.org/10.1590/S1679-78152013000700004

Kang J, Lv K, Sun Y, Li M (2025) Predictive risk assessment framework for leakage accident of offshore LNG transfer system. Expert Syst Appl 271: 126580. https://doi.org/10.1016/j.eswa.2025.126580

Khedmati MR, Pedram M (2014) A numerical investigation into the effects of slamming impulsive loads on the elastic-plastic response of imperfect stiffened aluminium plates. Thin Walled Struct 76: 118-144. https://doi.org/10.1016/j.tws.2014.04.008

Korobkin A, Khabakhpasheva T, Malenica S, Kim Y (2014) A comparison study of water impact and water exit models. Int. J. Nav. Archit. Ocean. Eng 6: 1182-1196. https://doi.org/10.1016/j.ijnaoe.2014.05.002

Liu B, Liu K, Villavicencio R, Dong A, Guedes Soares C (2021a) Experimental and numerical analysis of the penetration of welded aluminium alloy panels. Ships Offshore Struct 16(5): 492-504. https://doi.org/10.1080/17445302.2021.1947302

Liu B, Villavicencio R, Guedes Soares C (2014) On the failure criterion of aluminium and steel plates subjected to low-velocity impact by a spherical indenter. Int. J. Mech. Sci 80: 1-15. https://doi.org/10.1016/j.ijmecsci.2014.01.013

Liu B, Villavicencio R, Guedes Soares C (2015) Simplified analytical method to evaluate tanker side panels during minor collision incidents. Int. J. Impact Eng 78: 20-33. https://doi.org/10.1016/j.ijimpeng.2014.11.007

Liu B, Villavicencio R, Liu K, Zhu L, Guedes Soares C (2019) Response of an aluminium stiffened plate under extreme slamming loadings. J. Offshore Mech. Arct. Eng 141(5): 051606. https://doi.org/10.1115/1.4043159

Liu B, Villavicencio R, Zhang S, Guedes Soares C (2017) A simple criterion to evaluate the rupture of materials in ship collision simulations. Mar. Struct 54: 92-111. https://doi.org/10.1016/j.marstruc.2017.03.002

Liu B, Wang G, Chen BQ, Guedes Soares C (2021b) Experimental numerical and analytical analysis of the penetration of a scaled double-hull tanker side structure. Mar. Struct 78: 103018. https://doi.org/10.1016/j.marstruc.2021.103018

Liu B, Wang S, Villavicencio R, Guedes Soares C (2020) Slamming load and hydroelastic structural response of bow flare areas of aluminium fast displacement crafts. Ocean Eng 218: 108207. https://doi.org/10.1016/j.oceaneng.2020.108207

LR (2013) Guidance notes for the classification of special service craft. Lloyd's Register, London

LR (2020a) Rules and regulations for the classification of naval ships. Lloyd's Register, London

LR (2020b) Rules and regulations for the classification of special service craft. Lloyd's Register, London

LR (2020c) Rules for the manufacture, testing and certification of materials. Lloyd's Register, London

Lu J, Arnaud E, Sobey A (2019) Effective breadth for top-hat stiffened composite structures. Ocean Eng 196: 106841. https://doi.org/10.1016/j.oceaneng.2019.106841

Mutsuda H, Kanehira T, Kawawaki K, Doi Y, Yasukawa H (2018) Occurrence of stern slamming pressure and its characteristics in following irregular wave. Ocean Eng 170: 222-236. https://doi.org/10.1016/j.oceaneng.2018.10.046

Ojeda R, Prusty BG, Salas M (2004) Finite element investigation on the static response of a composite catamaran under slamming loads. Ocean Eng 31: 901-929. https://doi.org/10.1016/j.oceaneng.2003.11.004

Osborne M (2012) Single-element characterization of the LS-DYNA MAT54 material model. University of Washington, Seattle

Paik JK, Hughes OF, Hess PE, Renaud C (2006) Ultimate limit state design technology for aluminium multi-hull ship structures. SNAME Trans 113: 270-305

Paik JK, Shin YS (2006) Structural damage and strength criteria for ship stiffened panels under impact pressure actions arising from sloshing, slamming and green water loading. Ships Offshore Struct 1(3): 249-256. https://doi.org/10.1080/17445306.2006.10736501

Paik JK, Veen SVD, Duran A, Collette M (2005) Ultimate compressive strength design methods of aluminium welded stiffened panel structures for aerospace, marine and land-based applications: A benchmark study. Thin Walled Struct 43(10): 1550-1566. https://doi.org/10.1016/j.tws.2005.01.011

Qin Z, Batra RC (2009) Local slamming impact of sandwich composite hulls. Int J Solids Struct 46: 2011-2035. https://doi.org/10.1016/j.ijsolstr.2009.03.010

Ramos J, Guedes Soares C (1998) Vibratory response of ship hulls to wave impact loads. Int Shipbuild Prog 45(441): 71-87

Shabani B, Lavroff J, Davis MR, Holloway DS, Thomas GA (2019) Slam loads and pressures acting on high-speed wave-piercing catamarans in regular waves. Mar Struct 66: 136-153. https://doi.org/10.1016/j.marstruc.2019.03.002

Shin H, Seo B, Cho SR (2018) Experimental investigation of slamming impact acted on flat bottom bodies and cumulative damage. Int J Naval Architect Ocean Eng 10(3): 294-306. https://doi.org/10.1016/j.ijnaoe.2018.05.008

Swidan A, Thomas G, Ranmuthugala D, Amin W, Penesis I, Allen T, Battley M (2016) Experimental drop test investigation into wetdeck slamming loads on a generic catamaran hullform. Ocean Eng 117: 143-153. https://doi.org/10.1016/j.oceaneng.2016.01.020

Silva N, Wang S, Guedes Soares C (2020) ALE and finite element

investigation of water impact on composite panels. Guedes Soares (Ed.), Developments in the Collision and Grounding of Ships and Offshore Structures, Taylor and Francis Group, London, 227-236

Wang S, Guedes Soares C (2012) Analysis of the water impact of symmetric wedges with a multi-material Eulerian formulation. Int J Marit Eng 154(A4): 191-206. https://doi.org/10.3940/j.issn.2222-4266.2012.04.191

Wang S, Guedes Soares C (2013) Slam induced loads on bow-flared sections with various roll angles. Ocean Eng 67: 45-57. https://doi.org/10.1016/j.oceaneng.2013.01.018

Wang S, Guedes Soares C (2014) Comparison of simplified approaches and numerical tools to predict the loads on bottom slamming of ship structures. Guedes Soares C, Lopez Pena F (Eds.), Developments in Maritime Transportation and Exploitation of Sea Resources. Taylor & Francis Group, London, 157-170

Wang S, Guedes Soares C (2016) Experimental and numerical study of the slamming load on the bow of a chemical tanker in irregular waves. Ocean Eng 111: 369-383. https://doi.org/10.1016/j.oceaneng.2015.11.026

Wang S, Guedes Soares C (2017a) Hydroelastic analysis of a rectangular plate subjected to slamming loads. J Mar Sci Appl 16(4): 405-416. https://doi.org/10.1007/s11804-017-0009-4

Wang S, Guedes Soares C (2017b) Review of ship slamming loads and responses. J Mar Sci Appl 16(4): 427-445. https://doi.org/10.1007/s11804-017-0010-y

Wang S, Guedes Soares C (2020) Effects of compressibility, three-dimensionality and air cavity on a free-falling wedge cylinder. Ocean Eng 217: 107589. https://doi. org/10.1016/j.oceaneng.2020.107589

Wang JJ, Song YC, Wang W, Tu LF (2018) Evaluation of composite crashworthy device for pier protection against barge impact. Ocean Eng 169: 144-158. https://doi.org/10.1016/j.oceaneng.2018.05.016

Wang Y, Wu W, Wang S, Guedes Soares C (2020) Slam-induced loads of a three-dimensional bow with various pitch angles. J Offshore Mech Arctic Eng 142: 014502. https://doi.org/10.1115/1.4047116

Xu MC, Yanagihara D, Fujikubo M, Guedes Soares C (2013) Influence of boundary condition on the collapse behaviour of stiffened panels under combined loads. Mar Struct 34: 205-225. https://doi.org/10.1016/j.marstruc.2013.01.004

Yang B, Wu JM, Guedes Soares C, Wang DY (2018a) Dynamic ultimate strength of outer bottom stiffened plates under in-plane compression and lateral pressure. Ocean Eng 157: 44-53. https://doi.org/10.1016/j.oceaneng.2018.02.027

Yang B, Guedes Soares C, Wang DY (2018b) An empirical formulation for predicting the dynamic ultimate strength of rectangular plates under in-plane compressive loading. Int J Mech Sci 141: 213-222. https://doi.org/10.1016/j.ijmecsci.2018.04.022

Yu Z, Amdahl J, Grecoa M, Xu H (2019a) Hydro-plastic response of beams and stiffened panels subjected to extreme water slamming at small impact angles, part I: An analytical solution. Mar Struct 65: 53-74. https://doi.org/10.1016/j.marstruc.2018.11.004

Yu Z, Amdahl J, Grecoa M, Xu H (2019b) Hydro-plastic response of beams and stiffened panels subjected to extreme water slamming at small impact angles, part II: Numerical verification and analysis. Mar Struct 65: 114-133. https://doi.org/10.1016/j.marstruc.2019.01.004

Zha Y, Moan T (2001) Ultimate strength of stiffened aluminium panels with predominantly torsional failure modes. Thin Walled Struct 39(8): 631-648. https://doi.org/10.1016/S0263-8231(01)00011-0